buildings

MDPI

Article

Wind Flow Characteristics on a Vertical Farm with Potential Use of Energy Harvesting

Simeng Xie *, Pedro Martinez-Vazquez and Charalampos Baniotopoulos

Department of Civil Engineering, School of Engineering, University of Birmingham, Birmingham B15 2TT, UK; p.vazquez@bham.ac.uk (P.M.-V.); c.baniotopoulos@bham.ac.uk (C.B.)
* Correspondence: sxx366@student.bham.ac.uk

Abstract: The response to the climate emergency requires solutions that address multiple sustainability targets, which could be conducted by merging scientific research from areas that have traditionally evolved separately. This investigation presents advances in that direction by studying a building prototype designated for vertical farming, which enables the wind energy potential across built-up areas to be explored, in this case through the implementation of micro-wind turbines on the surface of the prototype. The study includes a parametric analysis consisting of varying locations of wind turbines across the building envelope, and the width of ventilation corridors. The effects of different widths of outdoor ventilation corridors, various locations, and additional wind angles on the capacity to harvest wind resources were investigated. The results showed that the 5 m wide outdoor corridor has the best ventilation effect, and the wind turbine placed on the roof has the best wind energy potential. The efficiency of wind turbines decreases significantly when multiple devices are placed at the same height on the façades, although overall, the potential for energy harvesting seems incremental.

Keywords: sustainable infrastructure; urban wind energy harvesting; vertical farming prototype; aerodynamic performance

Citation: Xie, S.; Martinez-Vazquez, P.; Baniotopoulos, C. Wind Flow Characteristics on a Vertical Farm with Potential Use of Energy Harvesting. *Buildings* **2024**, *14*, 1278. https://doi.org/10.3390/buildings14051278

Academic Editor: Fabio Rizzo

Received: 30 March 2024
Revised: 22 April 2024
Accepted: 29 April 2024
Published: 1 May 2024

1. Introduction

1.1. Vertical Farming and Urban Planning

Vertical farming, a modern agricultural cultivation method designed to solve the food problem caused by population growth, has proven to be an adequate agrarian production facility that can supply food to cities sustainably [1]. In the future, the integration of vertical farms (VFs) in urban planning will become the preferred solution for supplying fruits and vegetables to cities, fuelled by the shortage of energy resources and the lack of arable land due to rapid population growth [1,2]. At the same time, VFs are deemed to play a significant role in urban landscape architecture, adding value to buildings and a vehicle to generate technology and attract investment. In this process, the pace of the introduction of VFs into the modernization of cities will not stagnate.

The construction of VFs can enrich urban functionality and become a permanent source of oxygen and natural products. Prof. Dickson Despommier [2] included the concept of outdoor vertical planting corridors in his design of VFs, a critical approach to integrating VFs into urban planning. However, integrating outdoor planting corridors into high-rise building designs poses a significant challenge for the building's structure. The challenges include creating the building with openings that can safely interact with the wind, aerodynamical- and structural-wise, and ensuring that the facility can handle the plant volume to be stored in the outer corridors. Moreover, researchers have shown that urban vertical agriculture holds a significant portion of wind power [3], enabling electricity supply to the grid and adding resilience to the urban energy supply system. This paper develops a prototype for vertical farming and investigates its aerodynamic performance together with the energy resource that can be generated with micro-wind turbines distributed across the façade and roof.

In recent years, VFs have been criticized for requiring considerable initial investment and high amounts of electricity for operation and production compared to field production and greenhouses [3,4]. Ted Stathopoulos and his team [5] have suggested using wind turbines to harness wind energy in urban areas. Wind turbine design and building aerodynamics thus become an alternative for optimising the generation and utilisation of wind energy in cities. Wind energy resources stand as permanent and therefore lie at the core of a wealth of sustainable energy systems. Exploring the wind response characteristics of VFs and the application of wind energy thus becomes necessary for its correct implementation in modern urban construction. Amongst the various challenges to developing a suitable prototype is the fact that outdoor corridors of high-rise buildings need to house agricultural growing areas, which implies having openings across the building to allow proper interaction with the external environment. In solving the associated structural and aerodynamical problems induced by relatively large openings, one could focus on operational and management aspects, which are worth mentioning and align with various sustainability targets, as discussed later in this paper.

1.2. Research Gap and Objective

VFs lower the need for fresh air as indoor CO_2 concentrations reduce, which purifies particulate matter and volatile organic compounds, making them beneficial for interior environments [6]. On the other hand, the integration of flexible and multifunctional technologies within VFs may generate photovoltaic power [7], whereas a separate study [8] highlights that the potential benefits of operating vertical farming exceed the drawbacks, particularly regarding the ecological and health aspects. The drawbacks of outdoor and indoor VFs, which suffer from inadequate controllability and excessive energy use, contrast with their benefits [9,10]. While concept designs of multi-story VFs continue to develop, few modest multiple-story projects have been built or are currently under construction and will open for business soon. Table 1 shows examples.

Table 1. Cases of high-rise vertical farm buildings.

Case	Location	Height/m	Floor Count	Condition
Vertical Forest	Italy	112	28	Built
CapitaSpring	Singapore	276	51	Built
CapitaGreen	Singapore	245	40	Built
Oasia Hotel Downtown	Singapore	193.3	27	Built
Pasona Urban Farm	Japan	80	9	Built
DoubleTree by Hilton	UK	/	22	Ongoing
Vertical Forest	China	200	35	Ongoing
Farmscraper	China	218	51	Ongoing

Current research on VFs mainly concentrates on the design of the inside environment [11–13], auxiliary lighting systems [14,15], and energy consumption [3,4,16]. Not much work has been dedicated to structural design nor structure–wind interactions; the existing literature on high-rise building structural wind responses is based on office and residential structures. On the other hand, researchers have developed an interest in the wind energy potential of high-rise buildings [17], for example, through the implementation of duct openings that produce fennel effects, which could optimise wind energy harvesting [18,19] while improving building aerodynamics [20,21]. Existing works to assess wind energy potential and structural resilience of high-rise buildings use primarily CFD simulations [22,23] and wind tunnel tests [24,25]. CFD simulations are widely used to investigate the performance of wind energy devices, including rooftop wind catchers [26] and wind turbines [27]. With regards to experimental work, Fangwei et al. [28] developed a novel smart morphing façade system that modifies the aerodynamics of high-rise buildings and mitigates wind-induced vibrations.

The creation of high-rise buildings for agriculture has generated research on a variety of topics. For example, Vasiliki Pappa et al. investigated the aerodynamic effects of façade and roof greening on-air exchange from a cubic building [29]. Their experimental results demonstrated that the impact of the air exchange rate produced by façade greening is more prominent than that produced by roof greening. Neda Yaghoobian et al. [30] and E.A. Eumorfopoulou et al. [31], quantitatively assessed the effect of green roofs on the total energy balance and thermal performance of buildings. A separate study by Vahid Arabzadeh et al. [3] proposed urban vertical farming with large wind power share and optimised electricity costs, hence exploring the benefits of vertical farming for the decarbonisation of urban energy systems. In economic terms, George A. Xydis et al. [32] concluded that, in the worst-case scenario, the payback period of the small-scale Plant Factories with Artificial Lighting (ssPFAL) is 13 years, thus highlighting ssPFAL as a profitable investment. A study reported in [7] suggests the combination of small wind turbines and hydroponic systems to generate additional income and boost urban vegetable production, which could be attractive for the administrators of wind energy infrastructure. For the record, vertical farms can save energy and reduce emissions for cities, and several studies have been carried out on their own as a supply of urban agricultural products and on the potential of the vertical farming concept. However, there is a gap in the calculation of aerodynamic characteristics and the wind energy potential of high-rise vertical farms. If the wind energy potential of high-rise vertical farms can be researched and quantified, vertical farms could popularise in cities. Therefore, in this paper, wind turbines, which are used to improve the energy efficiency of buildings, are placed in vertical farms, and the effects of two variables, namely, the layout location and the number of arrangements, on the wind energy collection potential of vertical farms are compared.

For high-rise vertical farms, as agricultural buildings, the economic crop yields, and landscape value are enough to attract attention. But it is the undeniable wind energy potential that is the key attraction for architects and structural engineers. This paper presents a prototype of a high-rise VF hypothetically operating in an urban area. We use traditional CFD simulation techniques to determine the wind characteristics as well as their potential for clean energy harvesting. The wind flow characteristics discussed in this paper mainly include the wind pressure characteristics of the building façade, the trend of the flow velocity in the ventilation corridor, and the wind streamline around the building. The wind energy potential will be defined primarily by the amount of energy produced by wind turbines.

2. Methods

2.1. CFD Simulation

CFD Fluent (Ansys, Inc., Canonsburg, PA, USA) is a simulation method for mechanical analysis and validation of finite element models. CFD simulation tests are often applied in pre-project studies and when the possibility of undertaking full-scale experimentation is null. This study focuses on the CFD Fluent simulation of a building prototype with large outdoor planting corridors and micro-wind turbines attached to the walls. Past investigations have shown that vertical-axis wind turbines (VAWTs) activate with wind from any direction: therefore, these turbines do have yaw control mechanisms. Notwithstanding, horizontal axis wind turbines (HAWTs) have advantages over VAWTs in terms of high energy conversion, stability, controllability, reliability, and adaptability. Thus, HAWTs are generally better in extracting energy from wind than the VAWTs [33]. In this study, we model HAWTs with diameters of 15 m, which are usually preferred for operation in urban areas [34,35].

2.2. System Modelling

2.2.1. Modelling Parameters

Figure 1 shows the model developed for a vertical farm. It is 108 m tall, 80 m wide, and it has a chord of 60 m. The perimeter of the building fits an ellipsoid, and it has open outdoor corridors for planting and increased illumination. The floor height is 5.4 m and is proposed to use the 3rd, 6th, 9th, 12th, 15th, and 18th floors for vertical agricultural production.

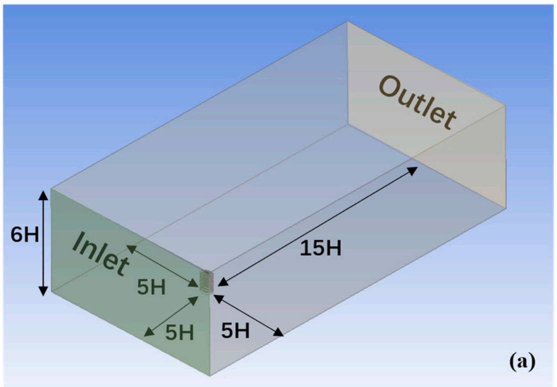

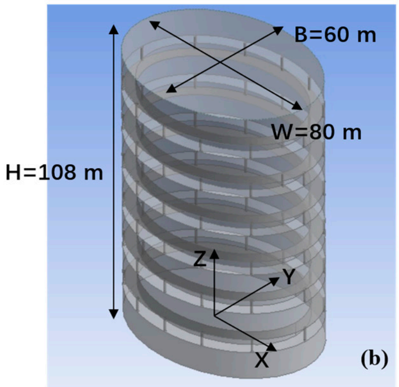

Figure 1. Overview of the benchmark: (**a**) computational domain, (**b**) building appearance.

The total volume rate of the "green area" in the vertical farm is 10.16% while the rest of the spaces are dedicated to supporting farming through operations, storage, and transport. According to [36] in the City of Birmingham, UK, the minimum per capita daily intake of fruits and vegetables is 0.4 kg; therefore, we estimate that one VF of this kind would be capable of supplying 1/6 of the green food demanded by its current population of 1.145 million [37]. Hence, to satisfy the entire demand for vegetables, the city would need to be equipped with 6 VFs of similar characteristics.

The building layout shown in Figure 1 has open outdoor corridors whose protection screens enable the penetration of wind. This configuration of façades is expected to induce aerodynamic effects that distinguish it from traditional buildings with little permeability to the airflow. To withstand wind loading, twelve structural columns are distributed across the floor system, whereas, to simulate the presence of shelves and ancillaries, blocks of 1.5 m wide and 1.5 m high were added to corridors. It is expected that such a configuration of elements will enable the assessment of turbulence levels and surface pressures across the building's structural and non-structural components. In this case, the Vestas V15 wind turbine was selected, and the blade structure was simplified appropriately for modelling purposes. Specific parameters are shown in Table 2, all the test subjects are equipped with this type.

Table 2. Specifications of wind turbines.

Type	Rated Power	Cut-in Wind Speed	Rotor Diameter	Swept Area
3 Blade HAWT	55 kW	4 m/s	15 m	176.625 m^2

2.2.2. Wind Velocity

The average wind profile was estimated with Equation (1), where u is the wind speed at height z, z_r is the reference height, u_r is the known wind speed at a reference height z_r, and α is the wind profile index, whose value is assumed of 0.3 [38].

$$u = u_r \left(\frac{z}{z_r} \right)^{\alpha} \tag{1}$$

According to the Wind Actions of Actions on Structures in Eurocode 1 [39], the basic velocity in Birmingham is around 22 m/s. Considering the influence of various environmental factors, 20 m/s is selected as the maximum design wind velocity for the study together with lower values having as a base those corresponding to daily wind.

When setting boundary conditions for CFD simulations, it is often necessary to estimate the intensity of turbulence at the inlet. There are a few cases of common estimations of the incoming turbulence intensity (TI): high (between 5% and 20%), medium (between 1% and 5%), and low (below 1%) turbulence case. Low turbulence cases are commonly used to describe the external airflow around cars, ships, submarines, and aircraft.

Turbulent kinetic energy is the average kinetic energy per unit of mass associated with eddies in turbulent flow. Figure 2 demonstrates the variation in turbulent kinetic energy with height and theoretical and simulation wind speed in different heights of the IV Terrain Category. The simulation results have a high similarity with the literature [40].

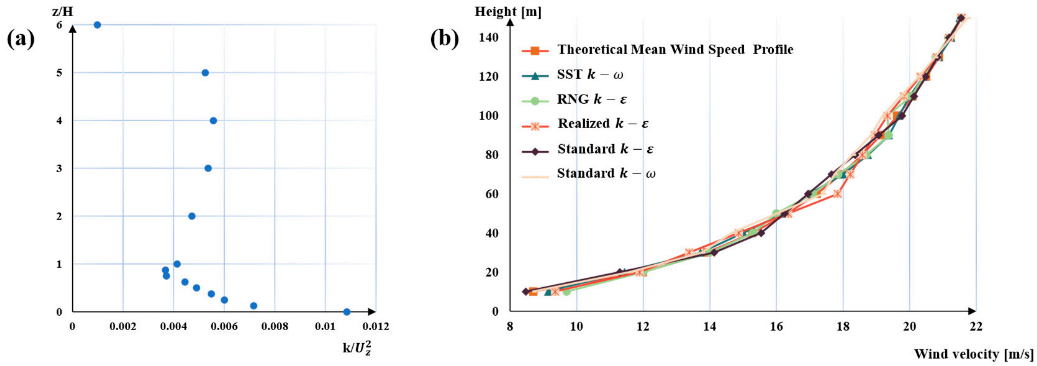

Figure 2. Inflow profile of the (**a**) turbulent kinetic energy and (**b**) theoretical and simulation wind speed in different heights of IV Terrain Category. k in (**a**) stands for turbulent kinetic energy, the theoretical wind speed profile in (**b**) is calculated by Equation (1), and the rest of the simulation results are calculated by ANSYS CFD 2023 R1.

3. Case Study

3.1. Computational Domain and Meshing

The simulations need to be set up with a reasonable balance between the discretisation of the mesh and accuracy. When wind flows through urban areas, it creates an aerodynamic effect around static objects as it encounters obstructions that modify the flow pattern. The windward area, where the flow stagnates, tends to receive a larger amount of energy. The energy imbalance compensates with flow detachment and reattachment depending on the size and geometry of structures.

When simulating wide-structure interactions within a wind tunnel, we observe some blocking effects due to the presence of physical boundaries imposed by the tunnel walls. This effect is characterized by the blocking rate $\rho_{blocking}$, which depends on the size of the building model and the cross-sectional area of the wind tunnel, as determined in Equation (2).

$$\rho_{blocking} = \frac{A_b}{A_d} \tag{2}$$

where A_b is the windward area of the building prototype and A_d is the cross-sectional area of the fluid domain. A similar blocking effect must be expected in a computational domain such as CFD [41–43].

When the blockage rate is less than 3% [42], it can be assumed that the obstruction effect does not interfere with the wind–structure interaction. Following previous studies [43], the length, width, and height of the computational domain are set to 20H + W, 10H + L, and 6H, where L, W, and H are the vertical farm's chord, width, and height, respectively. In the model adopted for this study, we calculate $\rho_{blocking-x} = 1.15\%$, and $\rho_{blocking-y} = 0.45\%$, for the x and y directions shown in Figure 1, respectively, which enabled the blocking effect in the computational domain to be disregarded.

With regards to the simulation domain, we established the outflow boundary where the rate of change in the flow direction is small enough as the outflow area is downstream of the position of the model, and the port is sloped. The outflow boundary should not affect the simulation solution. As shown in Figure 1a, the model was placed in the first one-third of the entire computational domain and close to the direction of the inlet, ensuring no backflow occurs at the outlet boundary.

3.2. Grid Independence Test

The grids are set unstructured. To ensure the accuracy of the test, it is necessary to try different grid sizes during a sensitivity analysis. To ensure the validity of the simulation results, we tried coarse, base, and fine grids of 1,309,804, 3,298,962, and 7,404,185 components, respectively. In such conditions, we calibrated the TI expected around the building envelope and inside corridors. The relative discrepancies obtained when comparing TI profiles by using coarse and base grids were 1.3%, while when using fine and base grids, we obtained a difference of 0.2%. This demonstrated that the base mesh does not affect the results.

The size of the meshing was set to 20 m in the outer flow domain, which changed to 1 m size in the neighbourhood of the surface of the vertical farm. This mesh configuration yielded an error below 2% when varying the number of grids. This simplified the number of running computations and facilitated convergence without compromising the accuracy of results. Table 3 shows the number of nodes and elements required, and some grid quality coefficients. The evaluation criteria selected for this study can be found in [44]. Figure 3 shows the accurate alignment of grid nodes at the connections as well as the level of grid refinement used to model the building.

Table 3. Grid Quality.

Type	Characteristic	Nodes	Elements	Element Quality	Aspect Ratio	Skewness	Orthogonal
Model 1	VF (No turbine)	604,576	3,298,962	0.82	1.90	0.25	0.75
Model 2	VF with Turbine 1	611,787	3,336,104	0.83	1.89	0.25	0.75
Model 3	VF with Turbine 2	674,202	3,688,788	0.82	1.90	0.25	0.75
Model 4	VF with Turbine ①~④	3,411,298	18,618,532	0.83	1.85	0.23	0.77

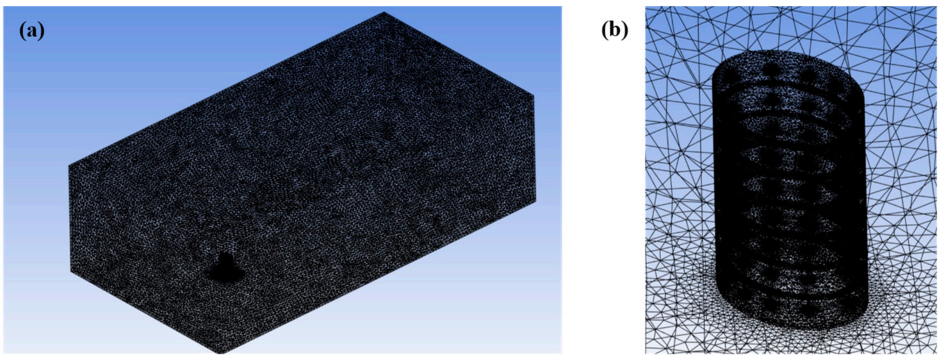

Figure 3. The meshing of (**a**) CFD Basin, and (**b**) example of the detailed mesh of Model 1.

3.3. Turbulence Method and Boundary Conditions

As the vertical farm is hypothetically located in Birmingham, we simulate the atmospheric boundary layer (ABL) corresponding to an urban area of such characteristics. To simulate turbulence in the ABL, we considered the $k-\varepsilon$ model, Realizable $k-\varepsilon$ model, RNG $k-\varepsilon$ model, $k-\omega$ model, and SST $k-\omega$ model, while acknowledging that none of these provides a definite solution as described in Table 4. This study includes micro-wind turbines attached to the building façade operating under a turbulent flow characteristic of an urban area; hence, we considered that the SST $k-\omega$ model is sufficient to stimulate the complex flow patterns across the façades and microturbine devices [45]. In other words, the SST $k-\omega$ model can meet the computational precision and accuracy required to capture the blade rotation of the wind turbine and the wind-driven response.

Table 4. Characteristics of different Turbulence models.

Type	Advantages	Disadvantages
Standard $k-\varepsilon$	The model has high stability, economy, and computational accuracy, is computationally reliable, has good convergence and low memory requirements.	The model uses wall functions, so viscous sub-layers and transition layers cannot be simulated, and it is only suitable for the simulation of fully turbulent flow processes.
Realizable $k-\varepsilon$	It performs well for rotating and boundary layer flows with strong adverse pressure gradients, separation, and secondary flows. The model suits various flow types.	Unphysical turbulent viscosity arises in calculations of flow fields with simultaneous stationary zones and rotation, such as multiple reference systems, rotating slip grids, etc.
RNG $k-\varepsilon$	The RNG theory provides an analytical formulation that considers the viscosity of low Noetherian flow. This enables the model to be more credible than the standard $k-\varepsilon$ model for a broader range of flows.	Only valid for fully developed turbulence, i.e., high Reynolds number turbulence models. Special treatment is needed for low Reynolds number flows and flows in the near-wall region.
Standard $k-\omega$	The model is widely applied for viscous simulations, general problems, internal flows, jet layers, large curvature flows, and separated flows, which can accurately represent wall behaviour.	The model only applies to laminar flow with parallel walls and has limitations in modelling turbulent flow, which is more challenging to converge than the $k-\varepsilon$ model. The results are sensitive to the initial conditions.
SST $k-\omega$	SST $k-\omega$ adapts the Standard $k-\omega$ model in the near-wall region and the $k-\varepsilon$ model in the area away from the wall. The model can better predict separation and reattachment.	The SST model sometimes converges slowly. Thus, the Standard $k-\omega$ or $k-\omega$ model must first be solved to obtain better initial conditions [46].

Utilising past preliminary testing and calibration, we set a maximum inlet velocity at 20 m/s and a turbulent intensity of 5%. In this way, the outlet pressure becomes 0 Pa for the established TI. Further flow parameters are given in Equation (3) (dissipation rate ω) and Equation (4) (turbulent kinetic energy).

$$\omega = C_\mu^{3/4}\frac{k^{3/2}}{l} \tag{3}$$

$$k = \frac{3}{2}(UI)^2 \tag{4}$$

In these equations, C_μ is the turbulence model constant, l is the turbulent length scale, U is the mean flow velocity, and I is the turbulence intensity, defined as follows:

$$I = \frac{u'}{U} \tag{5}$$

where u' is the root-mean-square of the turbulent velocity fluctuations defined as follows:

$$u' = \sqrt{\frac{1}{3}\left(u'^2_x + u'^2_y + u'^2_z\right)} = \sqrt{\frac{2}{3}k} \tag{6}$$

whereas the mean velocity U and turbulent viscosity μ_t can be calculated with Equations (7) and (8), respectively.

$$U = \sqrt{U_x^2 + U_y^2 + U_z^2} \tag{7}$$

$$\mu_t = \frac{\rho k}{\omega} \tag{8}$$

The rest of the walls in the computational domain are symmetrical and have no associated pressure wall conditions. The walls are free to slip, and solid walls with no slip are used at ground level and on the surfaces of the building, which means that if backflow occurs in the watershed, the total pressure is zero. Numerical simulations were carried out with the Couple solver for fluid–solid coupling and with a residual of 10^{-4}.

3.4. The Rotating Domain

The Fluent rotating domain allows flow dispersion in linear and rotational directions. In the study, the VF prototype is equipped with micro-wind turbines. Thus, the airflow around the turbine blades can be analysed. Allowing rotation is essential in our study as we want to estimate the amount of energy imparted by wind and that harvested by the microdevices. Hence, the Rotating Reference Frame (RRF) model was adopted to perform the analysis, so that the angular motion of the rotating equipment can be transformed into a non-rotating problem and thus simplify the numerical simulation of the fluid flow. The rotational angular velocity is set to 20 rad/min to couple the rotating domain with the external airflow. The Rotation-axis Origin and Direction are defined from the 3-D model data, according to the different positions of the wind turbines. To keep the blades rotating synchronously with the rotating domain, the boundary condition of the blades is assumed to be a Stationary Wall with an absolute velocity of zero relative to the adjacent cell zone (i.e., the rotating domain). This means that the rotating domain rotates with an angular velocity of 20 rad/min with respect to the global coordinate system, while the turbine blades are stationary with respect to the rotating domain. Meanwhile, the discretisation error could be minimised by applying the Absolute Velocity Formulation. The feature profile settings for the other non-rotated domains are the same as in Sections 3.1 and 3.3.

3.5. Validation

To ensure the accuracy of the experimental results, the design of the fluid domain, as described in the literature, was adopted in this investigation [43,47,48] for cases where there is no backflow at the outlet. To validate the model results, we compared the wind speeds recorded at different heights within the CFD domain, with theoretical values calculated with the power law profile presented in Section 2—see Figure 2b. Figure 2b elaborates on the comparison of wind flow determined with the five turbulence models pre-selected, namely, standard $k-\varepsilon$, Realizable $k-\varepsilon$, RNG $k-\varepsilon$, Standard $k-\omega$, and SST $k-\omega$. The curves obtained with SST $k-\omega$ give the best fit.

Furthermore, the pressure coefficients across the building envelope were compared against the recommendations given in the code of practice for wind-resisting design [39] for circular sections. To the authors' knowledge, buildings with ellipsoid features like the ones adopted here have not been studied before (neither numerically nor experimentally). Noting that, although the building prototype is not circular, the chord-to-width ratio of 0.75 would allow close similarities along the perimeter of the model, as shown in Figure 4a. Based on these results, we concluded that the CFD simulations are in close agreement with the theoretical values that were ultimately derived from field measurements.

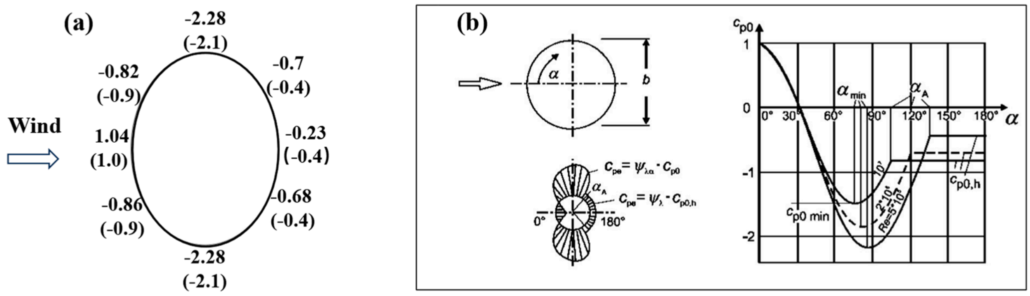

Figure 4. Profile of the (**a**) mean wind coefficients for the vertical farm benchmark (SST $k-\omega$ model) and (**b**) recommended external coefficients for circular cylinders. The values in the brackets in (**a**) are from (**b**), and (**b**) is from BS EN 1991-1-4-Wind actions [39]. Adapted with permission from EN 1991. Copyright year 2005, Copyright BSI (C).

4. Results

4.1. Wind Effects across Ventilation Corridors

To determine the pressure induced on the surfaces of planting racks located in the corridors, we modelled twelve cubic blocks of 3 m length, 3 m height, and 1.5 m width equispaced in each level. From Table 5, the maximum wind velocity in the corridor gradually increases with increasing height and reaches its maximum value at a height of H = 78.3 m, and the 5 m wide corridor would not induce significant changes to internal air circulation. In this study, the 5 m corridor is taken forward as it provides a better balance between the corridor area for farming and the internal layout that is destined for operation and services.

Table 5. Maximum velocity of 3 m, 4 m, 5 m, and 6 m width at each corridor height at inlet velocity = 20 m/s.

Height (m)	3 m Width	4 m Width	5 m Width	6 m Width
	Maximum Corridor Velocity (m/s)			
13.5	25.1554	24.4568	25.2314	24.8623
29.7	25.9653	26.1566	26.3596	25.7565
45.9	26.8535	26.7523	27.1547	26.6548
62.1	28.5268	28.3647	28.7635	28.1563
78.3	29.6478	29.7865	29.8629	29.1888
94.5	28.3657	28.1449	28.5585	28.2544

The maximum pressure occurs on the windward side of the plant rack closest to the velocity inlet (see Figure 5). As the wind gradually penetrates the sides of the vertical farm, the wind pressure on the surface of the shelves and columns decreases, which is predicted by the external pressure field shown in Figure 5. As discussed above, the outdoor corridor bears a large wind load due to the compression of the space, resulting in a large wind flow in the corridors. Yet, the ventilated planting corridors have good air circulation, and the placement of planting racks here ensures respiration and photosynthesis.

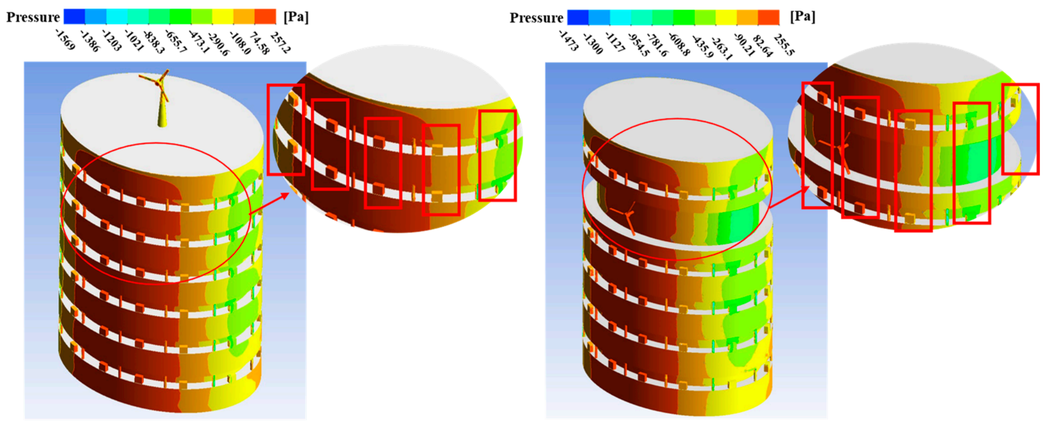

(a) Model 2 (b) Model 3

Figure 5. Pressure plots on the façade of (**a**) Model 2 and (**b**) Model 3 at inlet velocity of 20 m/s. The red squares identify the condition of plant racks.

4.2. Effect of Wind Turbine Arrangement Height

In the pre-experiment (see Figure 6), we observe that the velocity on the vertical and horizontal planes located 3 m away from the windward façade and 15 m above the roof did not decrease due to the roughness of the façade. Hence, to investigate the operational effectiveness of wind turbines placed across building façades, controlled tests were set up considering a 20 m tall wind turbine on the roof and one on the façade overhanging 3 m at a height of H = 78.3 m. The operating parameters of the wind turbine are given in reference [44]. Figure 7 illustrates the distribution of wind speeds at mid-corridor locations on the windward, leeward, and two sides of different heights. As stated in the Lawson comfort criteria [49], when wind speeds are greater than 10 m/s, people will feel uncomfortable; thus, cases with wind speeds less than 12.5 m/s are listed here. In practice, the annual average wind speed in Birmingham ranges from 4.7 to 5.5 m/s, with January being the windiest month, the average wind speed being 5.75 m/s. The probability of wind speeds exceeding 10 m/s in a year is less than 1 per cent [50]. When the wind passes through the ventilation corridor, its flow velocity increases significantly, and the maximum value of the wind velocity occurs between H = 62.1 m and H = 78.3 m, instead of increasing speed with increasing height. The possible reason for this is that the aerodynamic characteristics of high-rise ventilation corridors are strongly influenced by turbulence and building shape. The confusing turbulence caused a drop in wind velocity. On the trend, the height of the ventilation corridor affects wind speed and the ability of the wind turbine to harvest the wind energy. But the top corridor experiences a reduction in wind speeds. This can be attributed to unstable airflow from turbulence in the surroundings. This unstable airflow can lead to abrupt changes in wind speed, which increases the friction and resistance between the turbine blades and the airflow, thus reducing the efficiency and performance of the turbines.

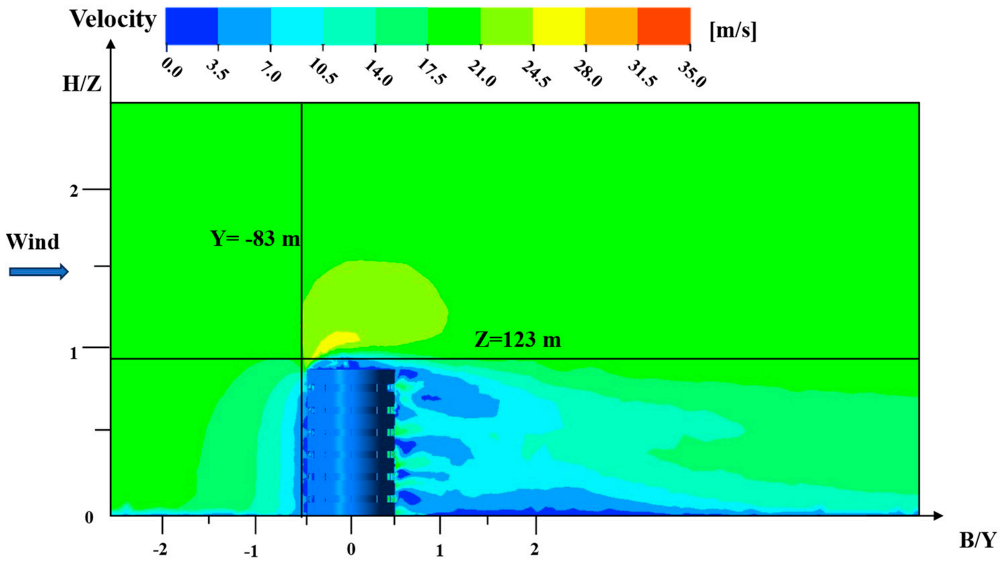

Figure 6. Diagram of velocity distribution around the vertical farm.

Figure 8 depicts the wind pressure coefficient plots around the turbines when the wind crosses the two heights (H = 78.3 m and H = 128 m); regardless of the height when the wind passes through the corridor, the speed decreases when it penetrates the blades, and the distribution is symmetrical along the central axis. The limitation of the results of this study is that the above results only consider the frontal windward (0°-wind) incidence and do not discuss the other wind attack angles. According to [44,51] and the results of this study, we can predict that the wind turbine on the windward side has the best performance when oriented perpendicular to the prevailing wind direction.

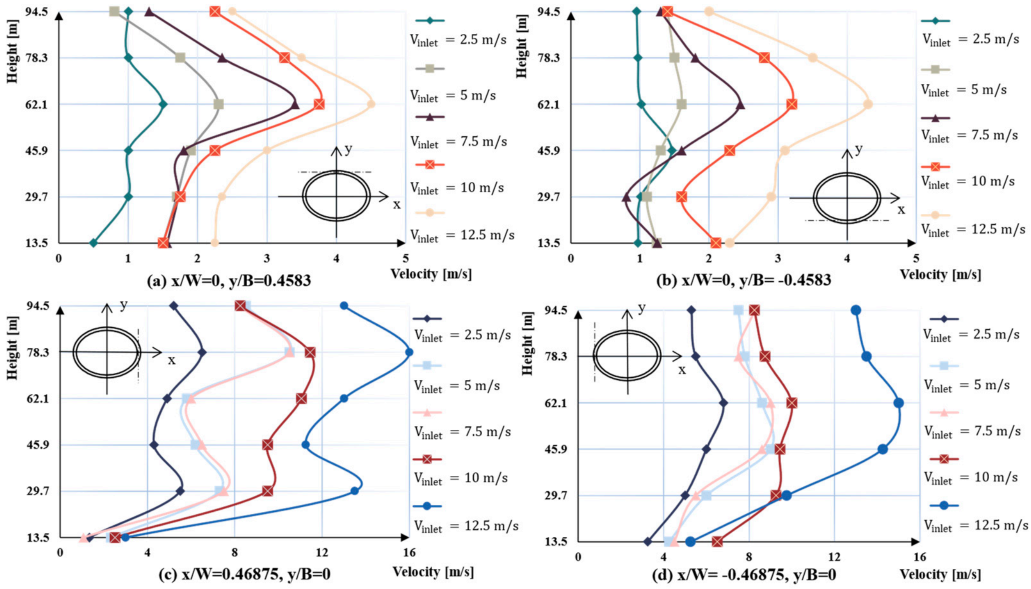

Figure 7. Wind velocity plot at (**a**) x/W = 0, y/B = 0.4583 (Leeward), (**b**) x/W = 0, y/B = −0.4583 (Windward), (**c**) x/W = 0.46875, y/B = 0 (Right), and (**d**) x/W = −0.46875, y/B = 0 (Left) of the building prototype with different inlet velocities at each central height of ventilation corridor.

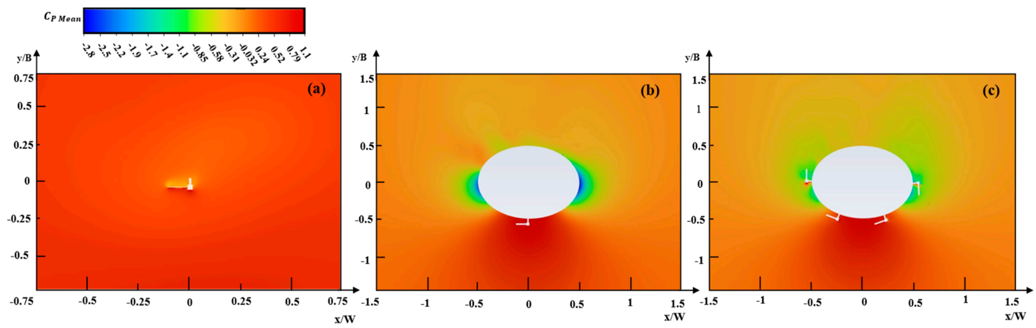

Figure 8. Wind pressure coefficients were recorded with (**a**) Model 2 at H = 128 m, (**b**) Model 3 and (**c**) Model 4 at H = 78.3 m at inlet velocity of 20 m/s.

4.3. Blades in Rotation Domain

To study the strength demand on blades and the surrounding flow field when the wind turbine is rotating, we simulated different configurations of wind turbines, which are shown in Figure 9. Model A has 1 WT on the roof, while Models B and C have 1 and 3 WTs on the façade, respectively. These models were subject to the wind flow by providing the blades of the WTs when they are static (Models 2–4 in Figure 10a–c) and with the ability to rotate (Figure 10d–f with the initial Model A–C). Figure 10 shows the blade pressure and velocity flow across all the models. The value of the pressure results from Figure 10 confirms that the pressure on the blade surface with the rotating domain is more prominent than that on the blade surface in a static position. The velocity trace distribution in Figure 10 shows that when the blades rotate, the wind flow around the vertical farm becomes more turbulent, hence imposing simultaneous strength demands/load-bearing capacity in various directions.

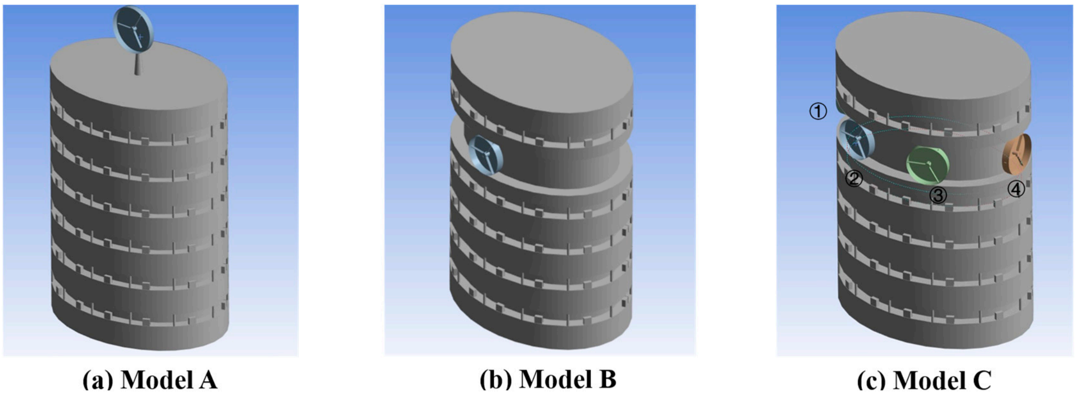

Figure 9. Models with rotation domain (**a**) Turbine 1 on the roof, (**b**) Turbine 2 at H= 78.3 m, and (**c**) Turbine ①~④ at H= 78.3 m.

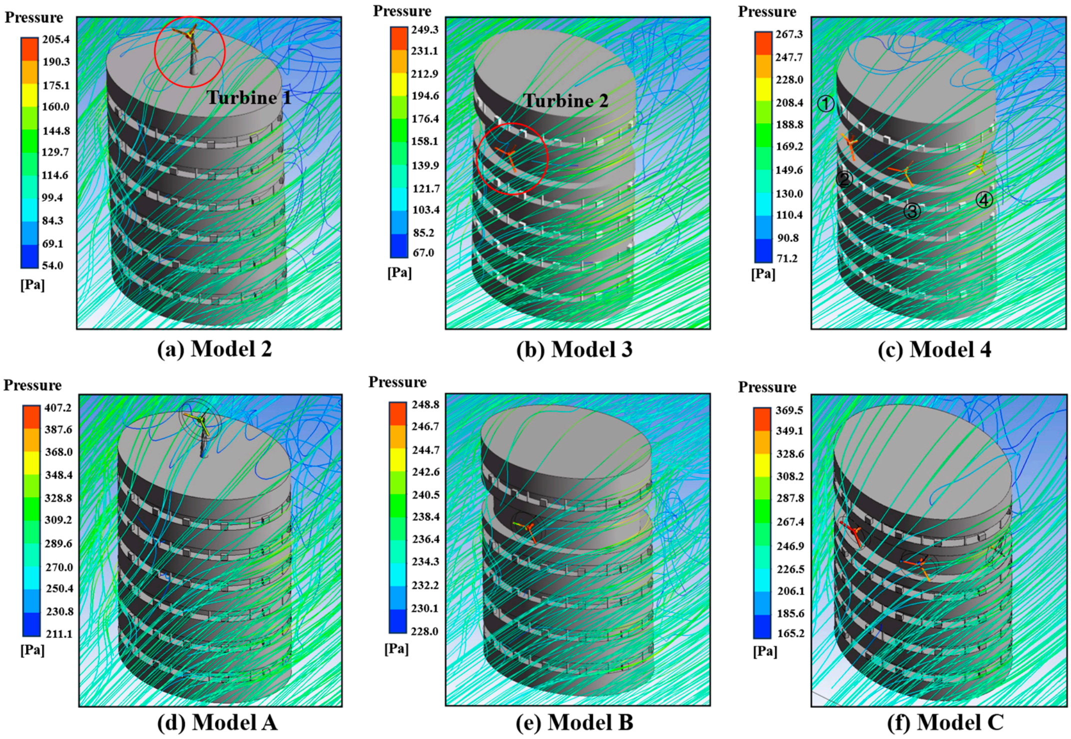

Figure 10. Wind streamlines and blade pressure distribution of models (**a**–**c**) with and (**d**–**f**) without rotation domain.

From the results in Figures 10 and 11 when the wind turbine blades rotate with a set rotation domain with an angular velocity of 20 rad/min, the absolute values of both the maximum positive and negative pressures on the surface of the blades increase, indicating that the airflow through the surface of the blades increases in speed and the distribution of the airflow becomes more complex. The blades used in this paper have a flat side and a curved side, the wind above the blades must travel around the longer curved side creating a lower pressure zone, while the wind below maintains the same pressure and thus becomes more pressurised than the wind above. Therefore, in future work, this pressure data can be used to optimise the design of the blades to improve the efficiency of the wind turbine, but this paper will not be concerned with the optimal design of blades.

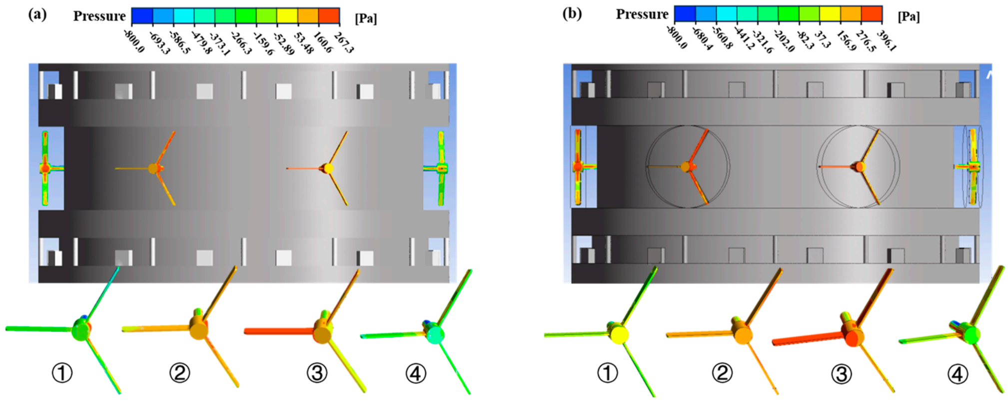

Figure 11. Wind pressure of models with four turbines (**a**) without rotation domain and (**b**) with rotation domain.

4.4. Potential Wind Energy Harvesting

Table 5 shows the results obtained at recording stations located at the height of H = 78.3 m where we see that the 5 m wide ventilation corridor has the best wind energy potential. This is because, within certain limits, wind is generated by the flow of air, and the larger the flow space, the relatively smaller the pressure of the airflow. However, as can be seen in Table 5, the maximum wind speed in the 6 m wide outdoor corridor is less than in the 5 m wide corridor. The outdoor corridor is narrow, and the airflow will naturally increase the internal pressure.

In this section, we scrutinise the potential for energy harvesting by considering two configurations of wind turbines:

(a) Two small wind turbines: Turbine 1 located on the roof and Turbine 2 located on the windward region of the façade.

(b) Four small devices: all turbines located on the façade as shown in Model C in Figure 10.

The potential wind energy of the wind turbines can be calculated from the wind energy formula (Equation (9)) bearing in mind that, according to Betz's Law, the wind turbine's ideal maximum energy utilisation factor is 0.593, which means the utilisation efficiency η is theoretically less than 0.593. To compare the leading wind energy captured by wind turbines under different inlet wind speed conditions, the electricity produced by the revolutions of each Turbine (1 and 2) in different inlet velocities is shown in Figure 12a.

$$E = \frac{0.5 \times \rho \times \mathrm{A} \times U^3 \times \eta}{1000} \tag{9}$$

where E denotes the theoretical wind energy (KW), ρ denotes the air density (Kg/m^3), A represents the effective area of the wind turbine blades (m^2), U denotes the wind speed (m/s), and η denotes the wind energy utilisation coefficient; here, we adopt the Betz's coefficients.

The start-up wind speeds for small wind turbines are typically in the range of 3–5 m/s. Under this wind speed, the fan will start automatically when it lasts for about 5–10 min, and the generator can start running. However, it must be recognised that wind speeds below 5 m/s are common in daily life and the energy potential of the wind turbines is marginal. Therefore, wind turbines can only be used as an auxiliary power supply system for vertical farming, and additional wind turbines need to be installed as appropriate. Since wind turbines operate at a low power level and their power supply capacity is largely dependent on the physical environment, the electricity generated by wind turbines can be used for night-time lighting of plant racks in ventilation corridors. These planting racks do not require daytime lighting and only require 8–12 h of night-time illumination. The illuminating power of industrial LED grow lights is usually 12–215 W [52]. Therefore, the electricity generated by wind turbines is well suited as a source of energy for lighting systems in planting racks.

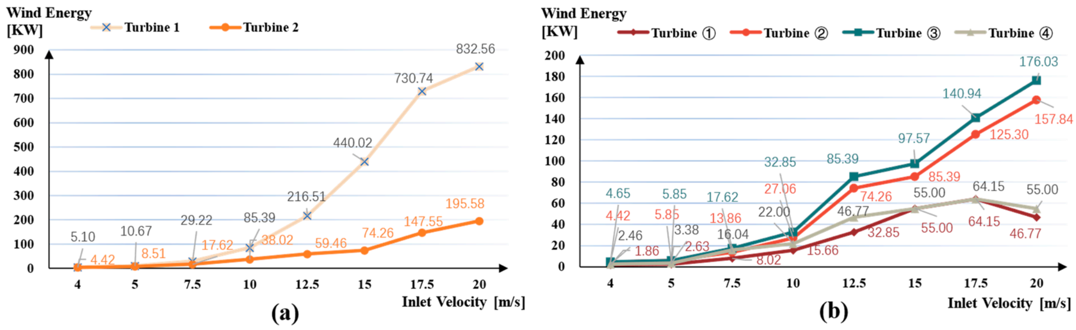

Figure 12. The theoretical maximum wind energy of (**a**) Turbine 1 and Turbine 2, and (**b**) Turbine ①~④ in different inlet velocities.

4.5. Effect of Wind Angle

Figure 12 shows that the number of wind turbine arrangements significantly affects the capacity of the wind turbine arrangement. In Figure 12b, we observe that the energy captured by Turbine ① and ④ with the same inlet speed is lower than that of Turbine ② and ③. In part, this is due to the misalignment of the axis of the nacelle with respect to the angle of attachment of the approaching wind, but also to the clustering of micro-wind devices on the façade. The relative difference in the potential for energy harvesting increases with the inlet velocity This means that wind turbines at the same height could produce different amounts of power due to different wind intensities and yaws with respect to the prevailing wind. Furthermore, turbulence effects also impact energy harvesting since the wind speed flowing through the surface of the wind turbines decreases, hence the output power. Designers will note that IEC 61400-1 [53] specifies the spacing requirements for different types of wind turbines, in which the spacing requirements for small wind turbines are limited to at least 1.5 to 2 times this ratio.

To investigate the optimal placement of the wind turbines on the building façade when the wind flows from the entrance to the vertical farm, Figure 10c shows that the four wind turbines with a rotating diameter of 15 m (wind angle of 60°) are uniformly arranged on H = 78.3 m of the vertical farm building, from left to right, and they are labelled Turbine ① to ④, respectively. The wind pressure distribution plots on the surface of the blades are shown in Figure 11a.

Figure 13a indicates that when the wind passes through the corridors on either side of the vertical farm, the turbulent kinetic energy is at its maximum. As Turbine ② and ③ are facing the windward inlet, and as the wind gradually flows to the wind turbines on both sides, the wind pressure on the surface of the wind turbine gradually decreases. From the XY plane velocity vector distribution of H = 78.3 m (Figure 13b), it can be learnt that the velocity size is symmetrically distributed with respect to the centreline of the building. The wind speed distribution around wind turbines ② and ③, which lie closer to the inlet of the velocity, is smaller than that of ① and ④. Therefore, the impeller obtains a more significant force. However, in the case of a wind turbine with the same rotational speed as the impeller, the higher the wind speed, the higher the power. Since the direction of the wind for wind turbines is constantly changing over time, wind turbines must face the prevailing wind to maximize the efficiency of wind energy. To maximise the utilisation of the wind turbines, these could have a tail fin.

From the experimental results so far, it can be seen that installing multiple wind turbines at the same height does lead to a reduction in individual wind collection potential, but the overall power generation potential of the wind turbine set is improved; this is because the direction of the incoming wind is variable, and setting up multiple sets of wind turbines can harvest winds from different directions, increasing the efficiency of the frontal winds; meanwhile, the Strata Building in London, UK, has been shown to provide around 8% of the building's energy from the three wind turbines mounted on top.

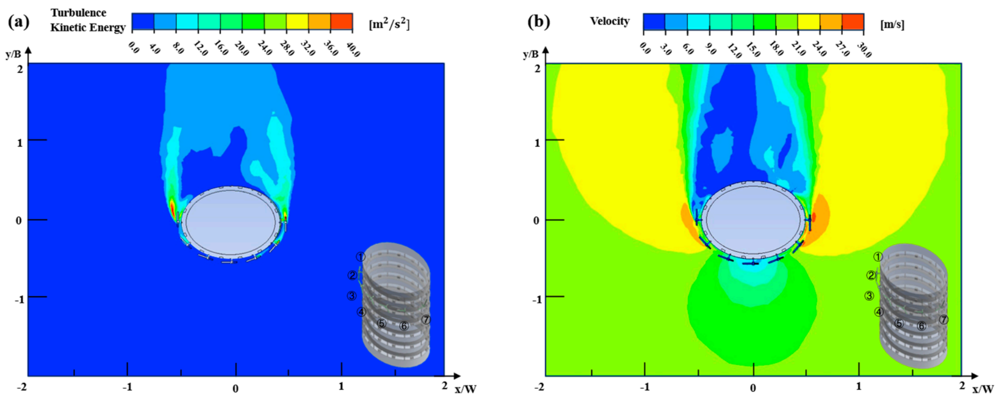

Figure 13. (**a**) Turbulence kinetic energy and (**b**) velocity plots in H = 78.3 m of Model 4.

5. Conclusions

This study focuses on the aerodynamic performance of a vertical farm model and its potential to harvest clean energy. To this end, we compared the impact of different widths of the outdoor corridor on the internal circulation of air and surface pressures induced on racks, the location of the wind turbine arrangement, and the windward direction of the wind turbines. The results obtained show that the vertical farm with 5 m wide outdoor corridors has the best performance. By comparing the wind pressure distribution on the surface of the wind turbine model and the variation in the surrounding flow field between the roof and the building façade, it is concluded that the wind turbine arranged on the roof can capture more wind energy. However, due to the influence of turbulence on the surface of the building, the rotating axis of the motor needs to be arranged at a height of more than 15 m above the roof, thus increasing the construction cost, which still needs to be considered in future planning.

The study (1) explored the wind energy potential of such buildings and whether this type of clean energy can be collected by effective means by proposing the construction of a vertical farm prototype; (2) analysed the distribution patterns of wind speed and wind pressure coefficients at different heights of the vertical farm, which provide reference data for the design of high-rise vertical farms and the introduction of urban planning; and (3) quantified the wind generation capacity of each set of wind turbines at different wind speeds of the vertical farm and compared their power generation potentials. The results indicate that vertical farming can be used to supply energy to the building itself in a sustainable way with wind power, but its power generation capacity is far from being able to meet its own demand. With full access to this clean energy source, the introduction of vertical farming into urban construction could undoubtedly be accelerated. Therefore, in future work, based on the physical characteristics of high-rise vertical farms, a variety of clean energy systems should be developed to efficiently collect clean wind energy and solve the problem of the high energy consumption of vertical farms, which will determine the future research direction.

Author Contributions: Conceptualization, P.M.-V. and S.X.; methodology, P.M.-V.; software, S.X.; validation, S.X., P.M.-V. and C.B.; formal analysis, S.X.; writing—original draft preparation, S.X.; writing—review and editing, P.M.-V.; supervision, C.B.; project administration, C.B. All authors have read and agreed to the published version of the manuscript.

Funding: This research was funded by China Scholarship Council, grant number 202308360083.

Data Availability Statement: The raw data, models that support the findings of this paper are available from the corresponding author upon reasonable request.

Conflicts of Interest: The authors declare that they have no known competing financial interests or personal relationships that could have appeared to influence the work reported in this paper.

References

1. Al-Chalabi, M. Vertical farming: Skyscraper sustainability? *Sustain. Cities Soc.* **2015**, *18*, 74–77. [CrossRef]
2. Despommier, D.D. *The Vertical Farm: Feeding the World in the 21st Century*, 1st ed.; Thomas Dunne Books/St. Martin's Press: New York, NY, USA, 2010.
3. Arabzadeh, V.; Miettinen, P.; Kotilainen, T.; Herranen, P.; Karakoc, A.; Kummu, M.; Rautkari, L. Urban vertical farming with a large wind power share and optimized electricity costs. *Appl. Energy* **2023**, *331*, 120416. [CrossRef]
4. Blom, T.; Jenkins, A.; Pulselli, R.; Dobbelsteen, A.v.D. The embodied carbon emissions of lettuce production in vertical farming, greenhouse horticulture, and open-field farming in the Netherlands. *J. Clean. Prod.* **2022**, *377*, 134443. [CrossRef]
5. Stathopoulos, T.; Alrawashdeh, H.; Al-Quraan, A.; Blocken, B.; Dilimulati, A.; Paraschivoiu, M.; Pilay, P. Urban Wind Energy: Some Views on Potential and Challenges. *J. Wind Eng. Ind. Aerodyn.* **2018**, *179*, 146–157. [CrossRef]
6. Shao, Y.; Li, J.; Zhou, Z.; Hu, Z.; Zhang, F.; Cui, Y.; Chen, H. The effects of vertical farming on indoor carbon dioxide concentration and fresh air energy consumption in office buildings. *Build. Environ.* **2021**, *195*, 107766. [CrossRef]
7. Tablada, A.; Kosorić, V. 11—Vertical farming on facades: Transforming building skins for urban food security. In *Rethinking Building Skins*; Gasparri, E., Brambilla, A., Lobaccaro, G., Goia, F., Andaloro, A., Sangiorgio, A., Eds.; Woodhead Publishing Series in Civil and Structural Engineering; Woodhead Publishing: Cambridge, UK, 2022; pp. 285–311.
8. Buscher, J.; Bakunowitsch, J.; Specht, K. Transformative Potential of Vertical Farming—An Urban Planning Investigation Using Multi-Level Perspective. *Sustainability* **2023**, *15*, 15861. [CrossRef]
9. Graamans, L.; Baeza, E.; van den Dobbelsteen, A.; Tsafaras, I.; Stanghellini, C. Plant factories versus greenhouses: Comparison of resource use efficiency. *Agric. Syst.* **2018**, *160*, 31–43. [CrossRef]
10. Park, J.E.; Kim, H.; Kim, J.; Choi, S.J.; Ham, J.; Nho, C.W.; Yoo, G. A comparative study of ginseng berry production in a vertical farm and an open field. *Ind. Crops Prod.* **2019**, *140*, 111612. [CrossRef]
11. Agati, G.; Franchetti, B.; Rispoli, F.; Venturini, P. Thermo-fluid dynamic analysis of the air flow inside an indoor vertical farming system. *Appl. Therm. Eng. Part B* **2024**, *236*, 121553. [CrossRef]
12. Sohn, J.; Liulys, M.; Avgoustaki, D.D.; Xydis, G. CFD analysis of airflow uniformity in a Shipping-Container vertical farm. *Comput. Electron. Agric.* **2023**, *215*, 108363. [CrossRef]
13. Ahamed, S.; Sultan, M.; Monfet, D.; Rahman, S.; Zhang, Y.; Zahid, A.; Bilal, M.; Ahsan, T.A.; Achour, Y. A critical review on efficient thermal environment controls in indoor vertical farming. *J. Clean. Prod.* **2023**, *425*, 138923. [CrossRef]
14. Avgoustaki, D.D.; Xydis, G. Energy cost reduction by shifting electricity demand in indoor vertical farms with artificial lighting. *Biosyst. Eng.* **2021**, *211*, 219–229. [CrossRef]
15. Cossu, M.; Tiloca, M.T.; Cossu, A.; Deligios, P.A.; Pala, T.; Ledda, L. Increasing the agricultural sustainability of closed agrivoltaic systems with the integration of vertical farming: A case study on baby-leaf lettuce. *Appl. Energy* **2023**, *344*, 121278. [CrossRef]
16. Pimentel, J.; Balázs, L.; Friedler, F. Optimization of vertical farms energy efficiency via multiperiodic graph-theoretical approach. *J. Clean. Prod.* **2023**, *416*, 137938. [CrossRef]
17. Gan, S.; Li, G.; Li, H. Assessment of wind energy potential within through-building openings under twisted wind flows. *Build. Environ.* **2023**, *244*, 110773. [CrossRef]
18. Zhong, H.-Y.; Jing, Y.; Sun, Y.; Kikumoto, H.; Zhao, F.-Y.; Li, Y. Wind-driven pumping flow ventilation of highrise buildings: Effects of upstream building arrangements and opening area ratios. *Sci. Total Environ.* **2020**, *722*, 137924. [CrossRef]
19. Hassanli, S.; Chauhan, K.; Zhao, M.; Kwok, K.C. Application of through-building openings for wind energy harvesting in built environment. *J. Wind Eng. Ind. Aerodyn.* **2019**, *184*, 445–455. [CrossRef]
20. Kaseb, Z.; Montazeri, H. Data-driven optimization of building-integrated ducted openings for wind energy harvesting: Sensitivity analysis of metamodels. *Energy* **2022**, *258*, 124814. [CrossRef]
21. Ruiz, C.A.; Kalkman, I.; Blocken, B. Aerodynamic design optimization of ducted openings through high-rise buildings for wind energy harvesting. *Build. Environ.* **2021**, *202*, 108028. [CrossRef]
22. Montazeri, H.; Montazeri, F. CFD simulation of cross-ventilation in buildings using rooftop wind-catchers: Impact of outlet openings. *Renew. Energy* **2018**, *118*, 502–520. [CrossRef]
23. Perén, J.; van Hooff, T.; Leite, B.; Blocken, B. CFD simulation of wind-driven upward cross ventilation and its enhancement in long buildings: Impact of single-span versus double-span leeward sawtooth roof and opening ratio. *Build. Environ.* **2016**, *96*, 142–156. [CrossRef]
24. Tominaga, Y.; Blocken, B. Wind tunnel analysis of flow and dispersion in cross-ventilated isolated buildings: Impact of opening positions. *J. Wind Eng. Ind. Aerodyn.* **2016**, *155*, 74–88. [CrossRef]
25. Zaki, A.; Sharma, R. Wind-tunnel analysis of turbulent flow in cross-ventilated buildings with windcatchers: Impact of surrounding buildings. *Build. Environ.* **2023**, *244*, 110826. [CrossRef]
26. Foroozesh, J.; Hosseini, S.; Hosseini, A.A.; Parvaz, F.; Elsayed, K.; Babaoğlu, N.U.; Hooman, K.; Ahmadi, G. CFD modeling of the building integrated with a novel design of a one-sided wind-catcher with water spray: Focus on thermal comfort. *Sustain. Energy Technol. Assess. Part C* **2022**, *53*, 102736. [CrossRef]

27. Ghorani, M.M.; Karimi, B.; Mirghavami, S.M.; Saboohi, Z. A numerical study on the feasibility of electricity production using an optimized wind delivery system (Invelox) integrated with a Horizontal axis wind turbine (HAWT). *Energy* **2023**, *268*, 126643. [CrossRef]
28. Hou, F.; Sarkar, P.P.; Alipour, A. A novel mechanism—Smart morphing façade system—To mitigate wind-induced vibration of tall buildings. *Eng. Struct. Part A* **2023**, *275*, 115152. [CrossRef]
29. Pappa, V.; Bouris, D.; Theurer, W.; Gromke, C. A wind tunnel study of aerodynamic effects of façade and roof greening on air exchange from a cubic building. *Build. Environ.* **2023**, *231*, 110023. [CrossRef]
30. Yaghoobian, N.; Srebric, J. Influence of plant coverage on the total green roof energy balance and building energy consumption. *Energy Build.* **2015**, *103*, 1–13. [CrossRef]
31. Eumorfopoulou, E.A.; Kontoleon, K.J. Experimental approach to the contribution of plant-covered walls to the thermal behaviour of building envelopes. *Build. Environ.* **2009**, *44*, 1024–1038. [CrossRef]
32. Xydis, G.A.; Liaros, S.; Avgoustaki, D.-D. Small scale Plant Factories with Artificial Lighting and wind energy microgeneration: A multiple revenue stream approach. *J. Clean. Prod.* **2020**, *255*, 120227. [CrossRef]
33. Al-Rawajfeh, M.A.; Gomaa, M.R. Comparison between horizontal and vertical axis wind turbine. *Int. J. Appl. Power Eng.* **2023**, *12*, 13–23. [CrossRef]
34. Cace, J.; ter Horst, R.E.; Syngellakis, H.K.; Power, I.T. *Urban Wind Turbines: Guidelines for Small Wind Turbines in the Built Environment*; RenCom: Ouderkerk aan de Amstel, The Netherlands, 2007; pp. 1–41.
35. Fan, X.; Ge, M.; Tan, W.; Li, Q. Impacts of coexisting buildings and trees on the performance of rooftop wind turbines: An idealized numerical study. *Renew. Energy* **2021**, *177*, 164–180. [CrossRef]
36. Caprile, A.; Rossi, R. 2021 International Year of Fruits and Vegetables; EPRS—European Parliamentary Research Service: 2021. Available online: https://www.europarl.europa.eu/RegData/etudes/ATAG/2021/689367/EPRS_ATA(2021)689367_EN.pdf (accessed on 17 January 2024).
37. Mid-Year Population Estimates, UK, June 2021. Office for National Statistics, 2022. Available online: https://www.ons.gov.uk/peoplepopulationandcommunity/populationandmigration/internationalmigration/bulletins/ukpopulationbycountryofbirthandnationality/yearendingjune2021 (accessed on 17 January 2024).
38. Dyrbye, C.; Hansen, S.O. *Wind Loads on Structures*; Wiley: New York, NY, USA, 1997.
39. *EN 1991*; Eurocode 1: Actions on Structures. British Standard: London, UK, 2006.
40. Zhang, S.; Du, B.; Ge, M.; Zuo, Y. Study on the operation of small rooftop wind turbines and its effect on the wind environment in blocks. *Renew. Energy* **2022**, *183*, 708–718. [CrossRef]
41. Li, J.; Guo, F.; Chen, H. A study on urban block design strategies for improving pedestrian-level wind conditions: CFD-based optimization and generative adversarial networks. *Energy Build.* **2024**, *304*, 113863. [CrossRef]
42. Badshah, M.; Van Zwieten, J.; Badshah, S.; Jan, S. CFD study of blockage ratio and boundary proximity effects on the performanceof a tidal turbine. *IET Renew. Power Gener.* **2019**, *13*, 744–749. [CrossRef]
43. Lee, Y.-T.; Lo, Y.-L.; Juan, Y.-H.; Li, Z.; Wen, C.-Y.; Yang, A.-S. Effect of void space arrangement on wind power potential and pressure coefficient distributions for high-rise void buildings. *J. Build. Eng.* **2023**, *75*, 107061. [CrossRef]
44. Xie, S.; Zheng, J.; Xiao, B.; Hu, H.; Cao, X.; Wang, X.; Zhang, L. Numerical Simulation and Wind Tunnel Test on the Wind-Induced Response of Three Typical Types of Greenhouse Main Structures. *Agriculture* **2022**, *12*, 1294. [CrossRef]
45. Arteaga-López, E.; Ángeles-Camacho, C.; Bañuelos-Ruedas, F. Advanced methodology for feasibility studies on building-mounted wind turbines installation in urban environment: Applying CFD analysis. *Energy* **2019**, *167*, 181–188. [CrossRef]
46. Zeng, Y.; Wang, H.B.; Sun, M.B.; Wang, C.; Liu, X. SST turbulence model improvements: Review. *Acta Aeronaut. Astronaut. Sin.* **2023**, *44*, 027411. (In Chinese)
47. Li, Y.; Zhu, Y.; Chen, F.-B.; Li, Q.-S. Aerodynamic loads of tapered tall buildings: Insights from wind tunnel test and CFD. *Structures* **2023**, *56*, 104975. [CrossRef]
48. Tominaga, Y.; Mochida, A.; Yoshie, R.; Kataoka, H.; Nozu, T.; Yoshikawa, M.; Shirasawa, T. AIJ guidelines for practical applications of CFD to pedestrian wind environment around buildings. *J. Wind Eng. Ind. Aerodyn.* **2008**, *96*, 1749–1761. [CrossRef]
49. Lawson, T.V. The wind content of the built environment. *J. Wind Eng. Ind. Aerodyn.* **1978**, *3*, 93–105. [CrossRef]
50. Windy.app. Available online: https://windy.app/forecast2/spot/9322/Birmingham (accessed on 17 January 2024).
51. Rivarolo, M.; Freda, A.; Traverso, A. Test campaign and application of a small-scale ducted wind turbine with analysis of yaw angle influence. *Appl. Energy* **2020**, *279*, 115850. [CrossRef]
52. Mills, T.; Dunn, B. LED grow lights for plant production. In *Oklahoma Cooperative Extension Service*; Oklahoma State University: Stillwater, OK, USA, 2016.
53. *IEC TC88-MT1/IEC 61400–1*; Wind Turbines—Part 1: Design Requirements. International Electrotechnical Commission: Geneva, Switzerland, 2005.